Tohoku J. Exp. Med., 2024, **263**, 227-238

Upregulation of Long Noncoding RNA MAGOH-DT Mediates TNF-*α* and High Glucose-Induced Endothelial-Mesenchymal Transition in Arteriosclerosis Obliterans

Kang-Jie Wang,[1,2,3,*] Yi-Xin Zhang,[2,4,*] Zhi-Wei Mo,[1,2,3,*] Zi-Lun Li,[1,2,3] Mian Wang,[1,2,3] Rui Wang,[1,2,3] Zhe-Cun Wang,[1,2,3] Guang-Qi Chang[1,2,3] and Wei-Bin Wu[1,2,3]

[1]Division of Vascular Surgery, The First Affiliated Hospital, Sun Yat-sen University, Guangzhou, Guandong, P.R. China
[2]National-Local Joint Engineering Laboratory of Vascular Diseases Treatment, The First Affiliated Hospital, Sun Yat-sen University, Guangzhou, Gunadong, P.R. China
[3]Guangdong Engineering Laboratoty of Diagnosis and Treatment of Vascular Disease, The First Affiliated Hospital, Sun Yat-sen University, Guangzhou, Guandong, P.R. China
[4]Division of Hypertension and Vascular Diseases, Department of Cardiology, Heart Center, The First Affiliated Hospital, Sun Yat-sen University, Guangzhou, Guandong, P.R. China

Arteriosclerosis obliterans (ASO) is characterized by arterial narrowing and blockage due to atherosclerosis, influenced by endothelial dysfunction and inflammation. This research focuses on exploring the role of MAGOH-DT, a long noncoding RNA, in mediating endothelial cell dysfunction through endothelial-mesenchymal transition (EndMT) under inflammatory and hyperglycemic stimuli, aiming to uncover potential therapeutic targets for ASO. Differential expression of lncRNAs, including MAGOH-DT, was initially identified in arterial tissues from ASO patients compared to healthy controls through lncRNA microarray analysis. Validation of MAGOH-DT expression in response to tumor necrosis factor-alpha (TNF-*α*) and high glucose (HG) was performed in human umbilical vein endothelial cells (HUVECs) using RT-qPCR. The effects of MAGOH-DT and HNRPC knockdown on EndMT were assessed by evaluating EndMT markers and TGF-*β*2 protein expression with Western blot analysis. RNA-immunoprecipitation assays were used to explore the interaction between MAGOH-DT and HNRPC, focusing on their role in regulating TGF-*β*2 translation. In the results, MAGOH-DT expression is found to be upregulated in ASO and further induced in HUVECs under TNF-*α*/HG conditions, contributing to the facilitation of EndMT. Silencing MAGOH-DT or HNRPC is shown to inhibit the TNF-*α*/HG-induced increase in TGF-*β*2 protein expression, effectively attenuating EndMT processes without altering TGF-*β*2 mRNA levels. In conclusion, MAGOH-DT is identified as a key mediator in the process of TNF-*α*/HG-induced EndMT in ASO, offering a promising therapeutic target. Inhibition of MAGOH-DT presents a novel therapeutic strategy for ASO management, especially in cases complicated by diabetes mellitus. Further exploration into the therapeutic implications of MAGOH-DT modulation in ASO treatment is warranted.

Keywords: arteriosclerosis obliterans; diabetes mellitus; endothelial-mesenchymal transition; inflammation; long noncoding RNA
Tohoku J. Exp. Med., 2024 August, **263** (4), 227-238.
doi: 10.1620/tjem.2024.J031

Received April 10, 2024; revised and accepted May 16, 2024; J-STAGE Advance online publication May 30, 2024

*These authors contributed equally to this work.
Wei-Bin Wu, M.D., Division of Vascular Surgery, The First Affiliated Hospital, Sun Yat-sen University, 58 Zhong Shan Er Road, Guangzhou, Guandong 510080, P.R. China.
e-mail: wuweib@mail2.sysu.edu.cn, wuweibsysu@163.com
Guang-Qi Chang, M.D., Ph.D., Division of Vascular Surgery, The First Affiliated Hospital, Sun Yat-sen University, 58 Zhong Shan Er Road, Guangzhou, Guandong 510080, P.R.China.
e-mail: changgq@mail.sysu.edu.cn

Introduction

Arteriosclerosis obliterans (ASO) is a common form of peripheral arterial disease (PAD), marked by the narrowing and blockage of major arteries due to atherosclerotic plaque formation, extending mainly from the abdominal aorta to the femoral arteries (Yuan et al. 2023). From a pathological vantage point, atherosclerosis is delineated as a chronic inflammatory pathology, significantly magnified by systemic risk factors such as hypertension, hypercholesterolemia, and hyperglycemia (Chen et al. 2021b; Zhao et al. 2022). To be specific, empirical evidence elucidates that inflammatory mediators, notably tumor necrosis factor-alpha (TNF-α), detrimentally affect endothelial integrity by precipitating the endothelial-mesenchymal transition (EndMT), a pivotal mechanism underlying vascular inflammation and the pathogenesis of atherosclerosis (Adjuto-Saccone et al. 2021; Chen et al. 2021a). Furthermore, studies underscores that exposure to elevated glucose levels constitutes a significant etiological factor for EndMT (Thomas et al. 2019; Lu et al. 2021). Although the induction of EndMT by inflammatory mediators and high glucose (HG) exposure occurs via disparate signaling cascades, a unifying aspect of their modulatory effects is the alteration in expression of transforming growth factor-beta (TGF-β), a potent effector of EndMT (Souilhol et al. 2018).

Long noncoding RNAs (lncRNAs), which are defined as a subset of noncoding RNAs exceeding 200 nucleotides in length with minimal protein-coding capacity, have been recognized for their pivotal role in the regulation of diverse cellular processes, influenced by extracellular signals (Collado et al. 2023). The involvement of lncRNAs in the pathophysiology of atherosclerosis has been increasingly substantiated by recent investigations. Notably, lincRNA-p21 has been identified as a critical modulator of neointima formation, vascular smooth muscle cell proliferation, apoptosis, and the progression of atherosclerosis (Wu et al. 2014). Similarly, SNHG12 has been documented to mitigate endothelial DNA damage-induced cellular senescence and atherosclerosis (Haemmig et al. 2020). Nonetheless, the precise roles and mechanistic pathways through which lncRNAs contribute to the advancement of ASO remain to be fully elucidated, indicating a significant gap in current understanding that warrants further explorative and investigative efforts.

In this study, we elucidated the upregulated lncRNA, designated as MAGOH divergent transcript (MAGOH-DT), within the arterial tissues of patients afflicted with ASO. Moreover, our data revealed that the concurrent stimulation of endothelial cells with TNF-α and HG levels precipitated an upsurge in MAGOH-DT expression, thereby catalyzing the EndMT. Significantly, our findings indicated that MAGOH-DT engages in molecular interactions with heterogeneous nuclear ribonucleoproteins C1/C2 (HNRPC), facilitating the binding of HNRPC to the mRNA of TGF-β2. This interaction subsequently elevated the expression of TGF-β2, further advancing the EndMT process. These insights unveiled a previously unrecognized therapeutic target for mitigating EndMT in ASO patients, particularly those presenting with hyperglycemia.

Materials and Methods

Sample acquisition

Arterial specimens from 18 patients diagnosed with ASO, who underwent major amputations, alongside venous blood samples, were procured at the First Affiliated Hospital, Sun Yat-sen University. Additionally, arterial samples from 6 healthy individuals, devoid of ASO, served as controls (see Supplementary Table S1). Following collection, arterial tissues were immediately frozen in liquid nitrogen and subsequently stored at −80°C for downstream analyses. Plasma, extracted from the venous blood, underwent assessments for TNF-α and glucose concentrations or was preserved at −80°C for future examination. The procurement of all samples was conducted with the informed consent of the participants. This study received the endorsement of the research ethics committee at the First Affiliated Hospital, Sun Yat-Sen University, adhering to the ethical guidelines of the Declaration of Helsinki (No. [2021]668).

Intimal RNA isolation from artery samples

RNA extraction from the intimal layer of artery samples was conducted following a method outlined in prior literature (Haemmig et al. 2020). Initially, the arteries were rinsed with phosphate-buffered saline (PBS, Gibco, Grand Island, NY, USA) to remove any residual blood or debris. The intimal layer was then carefully separated utilizing TRIzol reagent (Sigma-Aldrich, St. Louis, MO, USA), employing a sequential flushing technique: a 10-second flush of TRIzol (Sigma-Aldrich), a brief 10-second interval, followed by an additional 10-second flush. The material thus gathered was processed further to isolate RNA.

LncRNA microarray

The analysis of the Arraystar Human LncRNA Microarray V3.0 was carried out by Aksomics, Shanghai, China. Following the extraction and quantification of total RNA, rRNA was removed using the mRNA-ONLY™ Eukaryotic mRNA Isolation Kit (Epicentre, Madison, WI, USA). The RNA samples were then amplified and transcribed into fluorescent cRNA without 3' bias using the Arraystar Flash RNA Labeling Kit (Rockville, MD, USA), followed by purification, fragmentation, and heating. The cRNA was hybridized to the microarray slides, incubated at 65°C for 17 hours, fixed, and scanned with an Agilent DNA Microarray Scanner (G2505C, Santa Clara, CA, USA). Data were extracted using Agilent Feature Extraction Software, and lncRNA scatter plots were generated with RStudio. LncRNAs with normalized expressions > 7 in the ASO group and upregulated versus controls are listed in Supplementary Table S2.

Cell culture

Human umbilical vein endothelial cells (HUVECs, ScienCell, Carlsbad, CA, USA), human aortic smooth muscle cells (HASMCs, ScienCell), fibroblast cells (FBs, Juno, Guangzhou, China), and THP-1 monocytes (Procell, Wuhan, China) were acquired for the study. These cells were maintained in a controlled environment at 37℃ and 5% CO_2.

HUVECs were propagated in Dulbecco's Modified Eagle's Medium (DMEM, Gibco) supplemented with 10% fetal bovine serum (FBS, ScienCell) and 1% penicillin/streptomycin (P/S, ScienCell). For HG experiments, HUVECs received DMEM (Gibco) enriched with 4.5g/L D-glucose, alongside the standard 10% FBS (ScienCell) and 1% P/S (ScienCell).

HASMCs thrived in smooth muscle cell medium (SMCM, ScienCell), enhanced with 2% FBS (ScienCell), 1% smooth muscle cell growth supplement (ScienCell), and 1% P/S (ScienCell).

Fibroblast cells were cultured in DMEM (Gibco) with a supplement of 10% FBS (ScienCell) and 1% P/S (ScienCell).

THP-1 monocytes were grown in 1 × RPMI Medium 1640 (Gibco), containing 10% FBS (ScienCell) and 1% P/S (ScienCell). For differentiation into macrophages, THP-1 monocytes were treated with 100 ng/mL Phorbol 12-myristate 13-acetate (PMA, Sigma-Aldrich) for a duration of 48 hours.

RNA extraction, reverse transcription and RT-qPCR

RNA was isolated utilizing the Trizol reagent technique, and this isolated RNA was subsequently converted into complementary DNA (cDNA) employing the Transcriptor cDNA Synthesis Kit (Roche, Basel, Switzerland), following the protocols provided by the manufacturer. Real-time quantitative PCR (RT-qPCR) analyses were carried out with the LightCycler 480 SYBR Green I Master (Roche) on a Bio-Rad CFX96 platform (Hercules, CA, USA). In experiments involving HG exposure or diabetic conditions, the cycle threshold (Ct) values were adjusted based on the ACTB gene as an internal control. For other experimental conditions, the GAPDH gene served as the reference for normalization of Ct values. The sequences of the primers utilized for RT-qPCR are detailed in Supplementary Table S4.

Western blot

Western blot analysis was executed following established protocols (Mo et al. 2023). Cell lysis was achieved with RIPA buffer (Cell Signaling Technology, Danvers, MA, USA), and subsequent centrifugation facilitated the collection of supernatants for protein quantification. Proteins were then uniformly resolved via SDS-PAGE and electrotransferred onto PVDF membranes (Roche). These membranes underwent blocking in Tris-buffered saline (Boster, Wuhan, China) mixed with Tween-20 (Solarbio, Beijing, China) and 5% bovine serum albumin (BSA, Solarbio, Beijing, China) prior to an overnight incubation with primary antibodies. Following a series of washes, membranes were treated with HRP-linked secondary antibodies suitable for the primary antibodies used. Detection of protein bands was performed using the ECL chemiluminescence system (AI600, GE Healthcare, Little Chalfont, Buckinghamshire, UK). The study utilized primary antibodies targeting CD31 (3528, 1:1,000, Cell Signaling Technology), Ve-Cadherin (2500, 1:1,000, Cell Signaling Technology), α-SMA (ab7817, 1:1,000, Abcam, Cambridge, UK), Vimentin (5741, 1:1,000, Cell Signaling Technology), HNRPC (11760-1-AP, 1:5,000, Proteintech, Chicago, IL, USA), TGF-β2 (19999-1-AP, 1:1,000, Proteintech), phospho-Smad2/3 (8828, 1:1,000, Cell Signaling Technology), Smad2/3 (8685, 1:1,000, Cell Signaling Technology), and GAPDH (60004-1-Ig, 1:50,000, Proteintech).

Subcellular fractionation

The PARIS kit (Thermo Fisher Scientific, Waltham, MA, USA) was employed for the separation of nuclear and cytoplasmic fractions from cells, strictly adhering to the provided protocol. The process commenced with the collection and suspension of cells in cell fractionation buffer, maintained on ice for 10 minutes, followed by a 5-minute centrifugation to secure the cytoplasmic fraction. The nuclear pellet, once rinsed with the same buffer, was lysed using cell disruption buffer. Both cytoplasmic and nuclear extracts were then prepared by adding 2 × Lysis/Binding Solution and ethanol, respectively. RNA extraction proceeded via the filter cartridge, with subsequent washing steps using wash solutions 1 and 2/3. RNA was finally eluted by applying preheated elution solution at 95℃ through the filter cartridge membrane. The obtained cytoplasmic and nuclear RNAs were subjected to reverse transcription and RT-qPCR analyses.

ELISA assays

The concentration of TNF-α in plasma was determined through enzyme-linked immunosorbent assay (ELISA) techniques, utilizing the Human TNF-α ELISA Kit (CUSABIO, Wuhan, China) in strict accordance with the guidelines provided by the manufacturer.

Plasma glucose measurement

Fasting venous plasma glucose concentrations were assessed in the morning upon patient awakening, employing a blood glucose meter from Abbott Laboratories, Abbott Park, IL, USA, for the measurements.

Cell transfection

Small interfering RNAs (siRNAs) targeting specific sequences were custom-designed and produced by RiboBio, Guangzhou, China. For the transfection process, cells were introduced to these siRNAs employing the Lipofectamine RNAiMAX Transfection Reagent (Invitrogen, Carlsbad,

CA, USA), following the protocol specified by the manufacturer. The sequences addressed by these siRNAs are detailed in Supplementary Table S4.

EdU incorporation assays

The Cell-Light EdU Apollo567 In Vitro Kit (RiboBio) was utilized to perform 5-Ethynyl-20-deoxyuridine (EdU) incorporation assays, strictly adhering to the protocols outlined by the manufacturer. Prior to conducting these assays, HUVECs underwent transfection with siRNAs or were exposed to a combination of 100 ng/L TNF-α (NovoProtein, Suzhou, China) and HG. Following this preparatory step, the cells were incubated with 50 μM EdU for a duration of 8 hours. Cells were then fixed using 4% paraformaldehyde (PFA, Biosharp, Hefei, China) for 30 minutes, permeabilized with 0.5% Triton X-100 (Solarbio) for 20 minutes, and subsequently incubated with Apollo®567 dye for 30 minutes before being stained with Hoechst 33342 for an additional 30 minutes. Imaging was accomplished through a fluorescence microscope (Leica, Wetzlar, Germany), and the relative proliferation rate was determined by comparing the number of EdU-positive cells to the total cell count.

Transwell migration assays

Transwell migration assays were conducted in alignment with established methodologies (Zhang et al. 2010). In preparation for these assays, HUVECs underwent transfection with specific siRNAs or were pre-treated with a combination of 100 ng/L TNF-α (NovoProtein) and HG. The culture inserts, featuring 8.0 μm pore size PET track-etched membranes (Corning Incorporated, Corning, NY, USA), were pre-coated with 0.1% gelatin for an hour and subsequently blocked using 1% BSA (Solarbio) at 37°C for 30 minutes. The lower chamber of the Transwell setup was filled with DMEM (Gibco) enriched with 10% FBS (ScienCell). In the upper chamber, 5 × 10^4 cells per insert were seeded in DMEM (Gibco) diluted with 0.5% FBS (ScienCell) and allowed to migrate for 4 hours at 37°C. After migration, the cells were fixed using 4% PFA (Biosharp) for 15 minutes and stained with crystal violet for another 15 minutes. Cells that did not migrate through the membrane were gently wiped away from the upper side, leaving behind the cells that had successfully migrated, which were then documented and analyzed using a photomicroscope (Leica).

Tube formation assay

Tube formation assays were carried out in accordance with protocols outlined in previous studies (Li et al. 2020). As a preliminary step, HUVECs underwent either siRNA transfection or treatment with a mixture of 100 ng/L TNF-α (NovoProtein) and HG. The assay plates were prepared by coating them with Matrigel (Corning Incorporated) and incubating at 37°C for 30 minutes. Following this, each well received 1 × 10^5 cells, which were then incubated for an additional 4 hours at 37°C. The formation of tubular structures was documented using a photomicroscope (Leica), and the lengths of the tubes were quantified with the Image J software (NIH).

Immunofluorescence assay

Immunofluorescence staining was executed following established procedures (Mo et al. 2023). Cells were first fixed with 4% PFA (Biosharp) for 15 minutes and then permeabilized with 0.5% Triton X-100 (Solarbio) for 30 minutes. They were subsequently incubated with primary antibodies targeting CD31 (3528, 1:1,000, Cell Signaling Technology), VE-cadherin (2500, 1:400, Cell Signaling Technology), α-SMA (ab7817, 1:1,000, Abcam), or Vimentin (5741, 1:100, Cell Signaling Technology) overnight at 4°C. Following primary antibody incubation, the cells were treated with fluorophore-tagged secondary antibodies for one hour at ambient temperature and counterstained with 2-(4-Amidinophenyl)-6-indolecarbamidine dihydrochloride (DAPI, Abcam) to label nuclei. The stained specimens were then visualized and documented using a confocal laser scanning microscope (Nikon Eclipse Ni-E, Tokyo, Japan).

RNA pull down assays

Biotinylated RNA probes were developed and synthesized by Umine-bio, Guangzhou, China. Utilizing the Pierce™ Magnetic RNA-Protein Pull-Down Kit (Thermo Fisher Scientific), RNA pull-down assays were conducted following the manufacturer's protocol. Briefly, these probes were mixed with streptavidin magnetic beads at room temperature for 30 minutes to create probe-bead complexes, which were then incubated overnight with cell lysate at 4°C. The complexes were eluted, denatured, and the associated proteins were identified either through mass spectrometry or immunoblotting. Proteins binding specifically to MAGOH-DT, identified in mass spectrometry results post RNA pull-down, are detailed in Supplementary Table S3.

RIP assays

RNA-immunoprecipitation (RIP) assays were carried out with the Magna RIP™ RNA-Binding Protein Immunoprecipitation Kit (Millipore, Billerica, MA, USA), following the manufacturer's guidelines. The process involved incubating HNRPC antibody (Proteintech) or IgG with Protein A/G magnetic beads at room temperature for 30 minutes to create complexes. These complexes were then mixed with cell lysate overnight at 4°C. Afterward, total RNAs were isolated from the complexes and analyzed by RT-qPCR.

Statistical analysis

Data are reported as mean ± standard deviation (SD). Statistical evaluations were conducted utilizing SPSS version 13.0. For multiple group comparisons, significance was assessed via one-way ANOVA with Tukey's post-hoc

test or the Kruskal-Wallis test as appropriate. For two-group comparisons, significance was ascertained using the Student's t-test or the Mann-Whitney test, depending on data distribution. A P value of less than 0.05 was deemed significant. Further statistical information is detailed in the legends accompanying figures, within the main text, or in the methods section.

Results

HG and TNF-α increased MAGOH-DT expression in HUVECs

We performed a lncRNA microarray analysis to investigate the differential lncRNA transcriptome in the lower extremity arteries of patients with ASO compared to control subjects (Fig. 1A). 2,061 differentially expressed lncRNAs were detected [$|\log_2$Fold Change (normalized ASO/normalized Ctrl)$| > 1$]. We focused on the upregulated lncRNAs, because we aimed to silence these lncRNAs using oligonucleotide drugs as a potential therapeutic approach. Additionally, as low-abundance lncRNAs are often considered as non-functional (Palazzo and Lee 2015), we focused on lncRNAs with high abundance in the ASO group (Normalized expression > 7). We identified 512 lncRNAs for further analysis (Fig. 1A, B and Supplementary Table S2). Low-density lipoprotein receptor-related protein families (LRPs) have been found to be closely associated with atherosclerotic progression (Mineo 2020). Natural antisense lncRNAs often play a significant role in the pathological processes where their sense partners are involved (Li et al. 2008; Zhao et al. 2016; Krappinger et al. 2021). Thus, we determined to select natural antisense lncRNAs to LRPs for further studying its role in ASO. Notably, we found that lncRNA-MAGOH-DT gene partially overlaps in antisense to LRP8 gene (Fig. 1C). MAGOH-DT is a 1,181 nt lncRNA in National Center for Biotechnology Information (NCBI) database. We validated the expression of MAGOH-DT in different vascular cell types and found it was higher expression in HUVECs compared to HASMCs, FBs, and THP-1 macrophages, indicating its predominant expression in vascular endothelial cells (Fig. 1D). We further demonstrated that MAGOH-DT primarily localized to the nuclei of HUVECs by RT-qPCR analysis of the nuclear and cytoplasmic fractionations, which was confirmed by FISH assay (Fig. 1E, F). Inflammatory factors, HG and high lipid are common contributors to endothelial damage in ASO. To explore their relevance to MAGOH-DT expression in HUVECs, we treated HUVECs with TNF-α, HG or oxidized low-density lipoprotein (oxLDL) for 48 hours. RT-qPCR demonstrated that both TNF-α ($P < 0.001$) and HG ($P < 0.0001$) exposure increased MAGOH-DT expression in HUVECs, whereas oxLDL did not affect MAGOH-DT levels ($P > 0.05$) (Fig. 1G). Interestingly, the combined treatment of TNF-α and HG had a more significant effect on MAGOH-DT expression ($P < 0.0001$) (Fig. 1H). Moreover, RT-qPCR showed that MAGOH-DT levels was higher in the intima of lower extremity arteries in ASO patients compared to control subjects ($P < 0.01$), and in ASO patients with diabetes mellitus, MAGOH-DT was further upregulated ($P < 0.0001$) (Fig. 1I). The plasma levels of TNF-α ($r = 0.6064$, $P < 0.01$) and glucose ($r = 0.7052$, $P < 0.01$) were positively correlated with MAGOH-DT levels in the intima of ASO arteries (Fig. 1J, K).

MAGOH-DT regulated TNF-α/HG induced morphology change of endothelial cells

To confirm the regulatory effect of TNF-α/HG on MAGOH-DT in endothelial cells and investigate its relevance to endothelial function, we designed two different siRNAs to knock down MAGOH-DT in HUVECs (Supplementary Fig. S1). As shown in Fig. 2A-C, TNF-α/HG treatment significantly inhibited the proliferation, migration and tube formation of HUVECs (all $P < 0.0001$). However, transfecting HUVECs with MAGOH-DT siRNAs did not recover these endothelial functions ($P > 0.05$). Moreover, we found that TNF-α/HG treatment induced transition in cellular morphology from cobblestone-like shape to an elongated spindle-shaped form, which is the characteristic of EndMT, whereas knocking down MAGOH-DT effectively recovered endothelial cells morphology (Fig. 2D). We drew from these data that MAGOH-DT might play a role in TNF-α/HG induced EndMT.

TNF-α/HG induced EndMT by upregulating MAGOH-DT

To further elucidate whether MAGOH-DT is involved in TNF-α/HG-induced EndMT, we detected the expression of EndMT markers. In the present study, we confirmed that TNF-α/HG treatment could not only downregulate the expression of endothelial markers CD31 and VE-cadherin but also upregulate the expression of mesenchymal markers α-SMA and Vimentin (all $P < 0.001$) (Fig. 3A, B). However, when MAGOH-DT was knocked down in the HUVECs, the downregulation of CD31 and VE-cadherin, as well as the upregulation of α-SMA and Vimentin, were reversed (all $P < 0.05$) (Fig. 3A, B).

In order to evaluate the role of MAGOH-DT on TNF-α/HG-induced EndMT, we performed immunofluorescence staining. As shown in Fig. 3C, D, TNF-α/HG induced HUVECs to transform into elongated spindle-shape accompanied with changes of cell markers, whereas transfecting HUVECs with MAGOH-DT siRNAs effectively recovered the morphology and cell markers of endothelial cells (all $P < 0.01$). Furthermore, MAGOH-DT levels were negatively correlated with CD31 mRNA levels ($r = -0.7018$, $P < 0.01$) and positively correlated with α-SMA mRNA levels ($r = 0.8180$, $P < 0.0001$) in the intima of ASO arteries (Fig. 3E, F), which indicated that MAGOH-DT levels was positively correlated with degree of EndMT in the arteries. These findings suggest that TNF-α/HG-induced upregulation of MAGOH-DT in HUVECs contributes to the induction of EndMT.

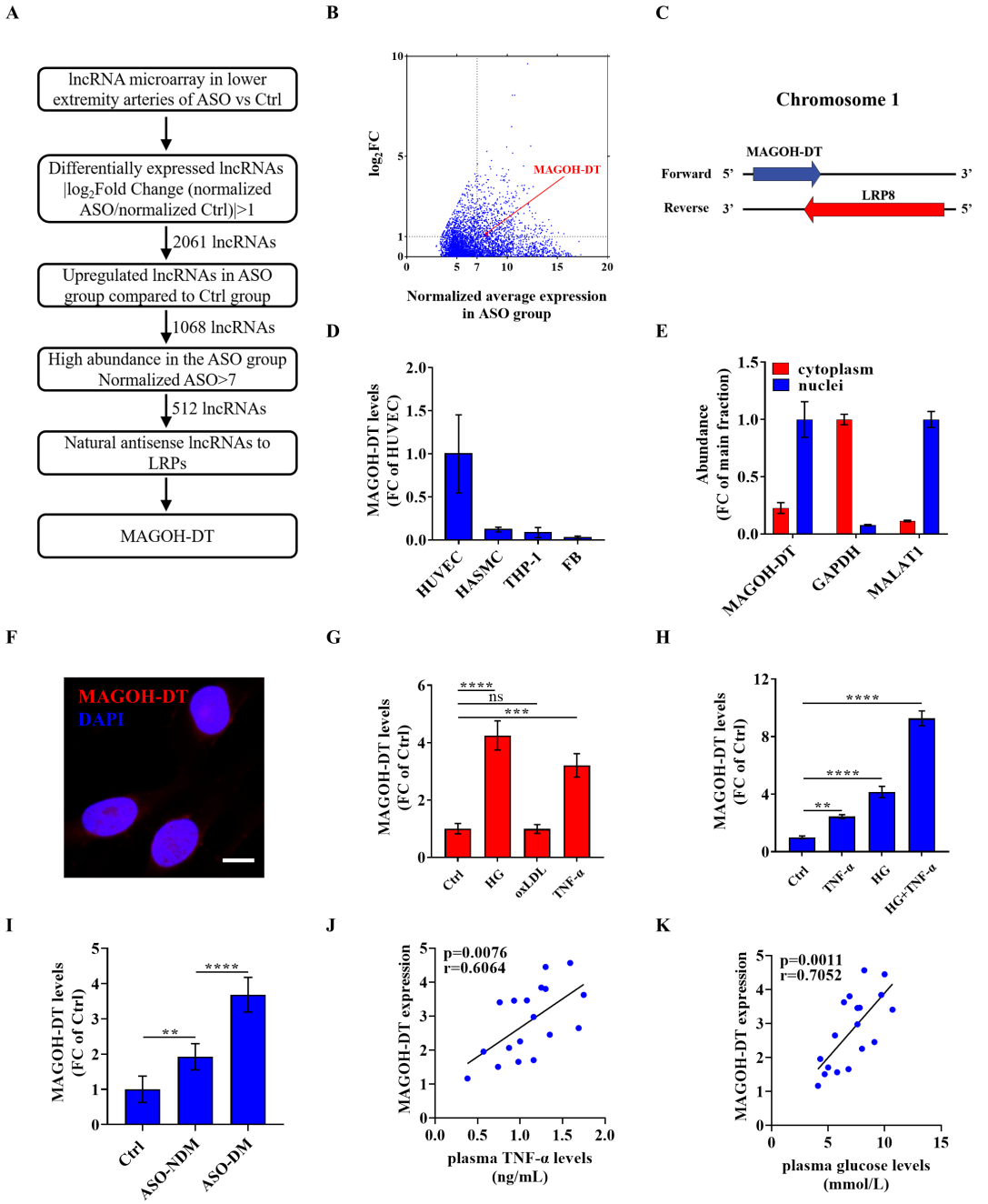

Fig. 1. HG and TNF-α increased MAGOH-DT expression in HUVECs.
A. Selection strategy for lncRNAs in lower extremity arteries of ASO and control patients. B. Scatter plot of upregulated lncRNAs in the lower extremity artery between ASO patients and healthy individuals. C. Illustration of the gene localization of MAGOH-DT and LRP8. D. RT-qPCR was used to determine the MAGOH-DT levels in different types of vascular cells, including HUVECs, HASMCs, THP-1 macrophages (THP-1 cells) and fibroblasts (FBs). E. RT-qPCR was used to determine the subcellular abundance of MAGOH-DT. F. The subcellular location of MAGOH-DT (red) in HUVECs was determined by FISH. Scale bars, 10 μm. G. RT-qPCR confirmed MAGOH-DT expression in HUVECs treated with high glucose (HG), oxidized low-density lipoprotein (oxLDL, 50 μg/mL) or TNF-α (100 ng/mL). H. RT-qPCR confirmed MAGOH-DT expression in HUVECs treated with HG, TNF-α, or both. I. RT-qPCR confirmed MAGOH-DT expression in the arterial endothelium of control subjects (n = 6) and ASO patients with (n = 6) or without (n = 6) diabetes mellitus. J. Correlation between plasma TNF-α levels and MAGOH-DT levels in the ASO arterial endothelium (n = 18). K. Correlation between plasma glucose levels and MAGOH-DT levels in the ASO arterial endothelium (n = 18). ASO-NDM, ASO patients without diabetes mellitus; ASO-DM, ASO patients with diabetes mellitus. For D-H, n = 3 independent experiments; $^{**}P < 0.01$; $^{***}P < 0.001$; $^{****}P < 0.0001$; ns, not significant.

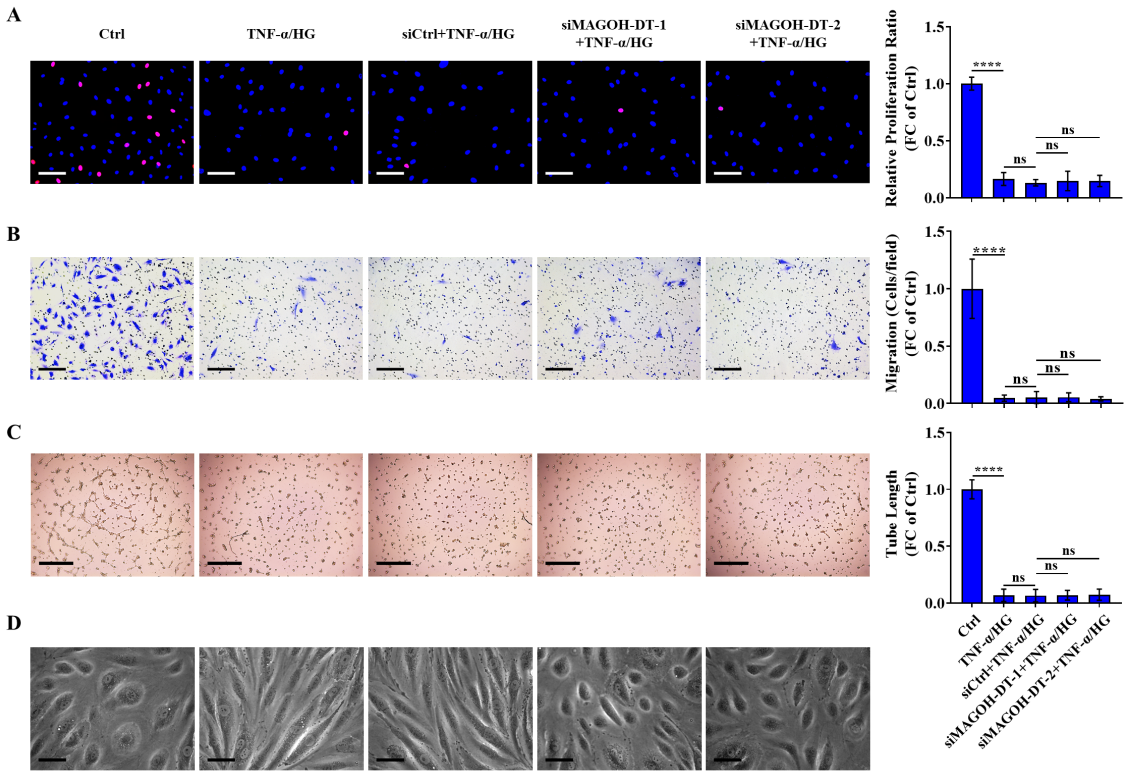

Fig. 2. MAGOH-DT regulated TNF-α/HG-induced morphological changes in endothelial cells.
A. Representative images (left) and quantification (right) of EdU incorporation in HUVECs treated with TNF-α (100 ng/mL) plus HG for 48 h after knocking down MAGOH-DT. Scale bars, 100 μm. B. Representative images (left) and quantification (right) of transwell migration assays of HUVECs treated with TNF-α (100 ng/mL) plus HG for 48 hours after knocking down MAGOH-DT. Scale bars, 100 μm. C. Representative images (left) and quantification (right) of tube formation assays of HUVECs treated with TNF-α (100 ng/mL) plus HG for 48 hours after knocking down MAGOH-DT. Scale bars, 500 μm. D. Representative images of morphological changes in HUVECs treated with TNF-α (100 ng/mL) plus HG for 48 hours after MAGOH-DT was knocked down. Scale bars, 50 μm. For all the assays, n=3 independent experiments were performed. ****$P < 0.0001$; ns, not significant.

TNF-α/HG upregulated MAGOH-DT to promote TGF-β2 translation by promoting the interaction between HNRPC protein and TGF-β2 mRNA

To investigate the mechanism of TNF-α/HG-induced MAGOH-DT upregulation in EndMT, we conducted RNA pull-down assays followed by mass spectrometry. We identified 132 proteins that specifically bound to MAGOH-DT (Fig. 4A and Supplementary Table S3). Notably, HNRPC was the top enriched protein (ranked by emPAI) with a high protein score (Fig. 4B). The interaction between MAGOH-DT and HNRPC in HUVECs was confirmed using RNA pull-down assays and RIP ($P < 0.0001$) (Fig. 4C, D). Previous studies indicates that HNRPC is involved in cell proliferation and differentiation, but its effect on EndMT remains unclear (Panchenko et al. 2009).

TGF-β is a crucial regulator of EndMT (Xiao and Dudley 2017; Ma et al. 2020; Alvandi and Bischoff 2021). Mammalian TGF-β consists of three isoforms: TGF-β1, TGF-β2 and TGF-β3, and all of them have been reported to induce EndMT in human endothelial cells (Hong et al. 2020; Ciavarella et al. 2021; Nasim et al. 2023). HNRPC is a nuclear-restricted RNA-binding protein involved in mRNA stability, splicing, export and translation (Mo et al. 2022; Dantsuji et al. 2023). Previous studies show that HNRPC preferably binds to continuous uridine tracts (U-tracts) of nine or more uridines (Cieniková et al. 2014, 2015). Both of TGF-β2 and TGF-β3 contain multiple consecutive uridine fragments that correspond to the HNRPC binding motif (Fig. 4E). Thus, we investigated whether TNF-α/HG-induced MAGOH-DT regulated the interaction between HNRPC protein and TGF-β mRNAs. We performed RIP-RT-qPCR and found that HNRPC protein bound to TGF-β2 mRNA in HUVECs ($P < 0.0001$), but not to TGF-β1 or TGF-β3 ($P > 0.05$) (Fig. 4F). Moreover, neither TNF-α/HG treatment nor MAGOH-DT and HNRPC siRNAs affected TGF-β2 mRNA levels (all $P > 0.05$) (Fig. 4G and Supplementary Fig. S2A). However, at the protein levels, TNF-α/HG treatment significantly upregulated TGF-β2 in HUVECs, which was attenuated by knocking down MAGOH-DT, HNRPC or both (all $P < 0.0001$) (Fig. 4H and Supplementary Fig. S2B). Previous studies indicates that HNRPC is a RNA binding protein that can increase mRNA translation by binding to its 3′-UTR. These results suggest that TNF-α/HG increases MAGOH-DT expression

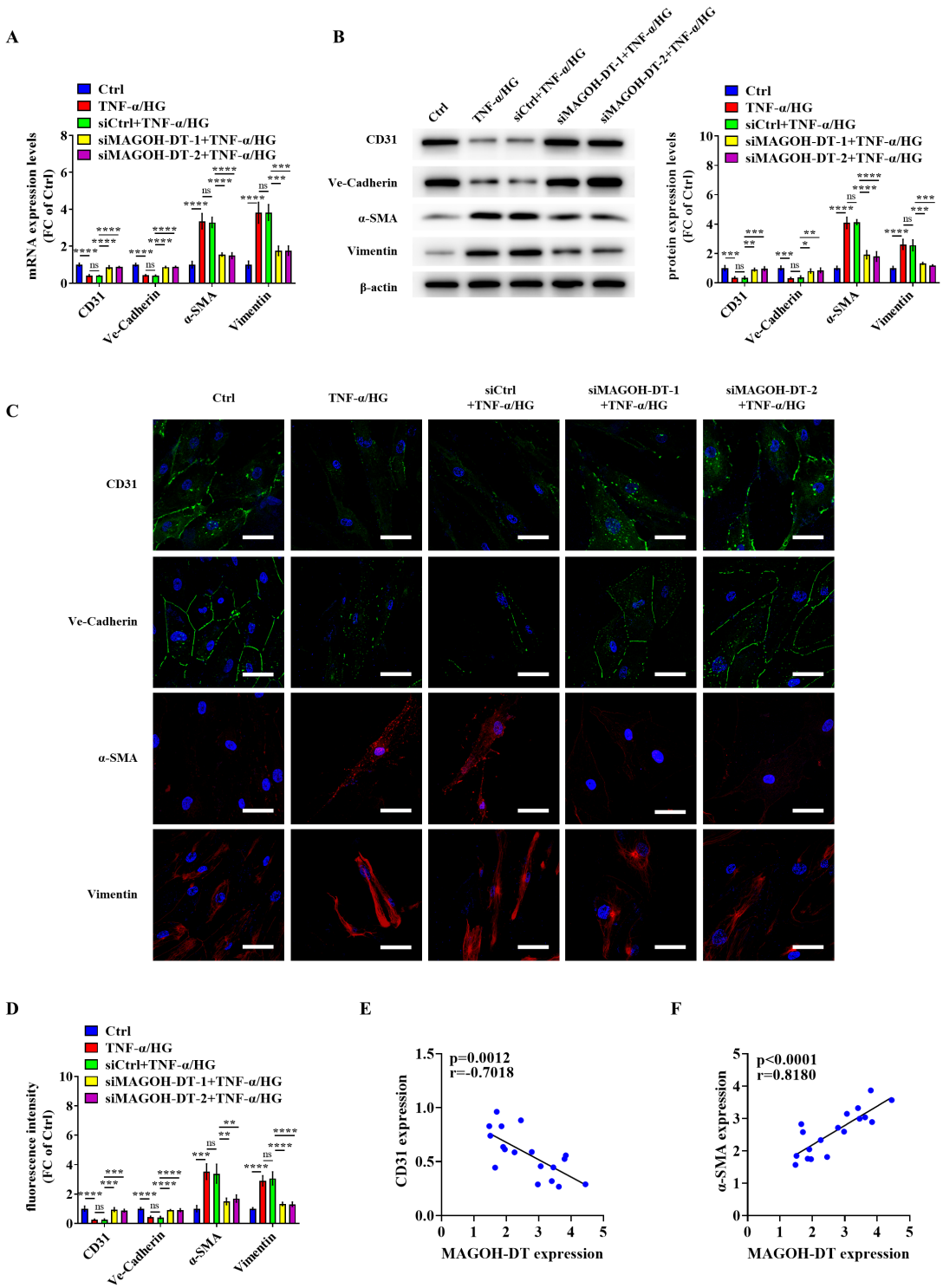

Fig. 3. TNF-α/HG induced EndMT by upregulating MAGOH-DT.
A. RT-qPCR was used to determine the mRNA levels of CD31, VE-cadherin, α-SMA, and Vimentin in HUVECs treated with TNF-α (100 ng/mL) plus HG for 48 hours after knocking down MAGOH-DT. B. Western blot analysis of CD31, VE-cadherin, α-SMA and vimentin in HUVECs treated with TNF-α (100 ng/mL) plus HG for 48 hours after knocking down MAGOH-DT. Representative plots (left) and quantification (right) are shown. C, D. HUVECs treated with TNF-α (100 ng/mL) plus HG for 48 hours after MAGOH-DT knockdown were analyzed by immunofluorescence for the expression of CD31, Ve-cadherin, α-SMA, and Vimentin. Representative images (C) and quantification (D) are shown. Scale bars, 50 μm. E. Correlations between MAGOH-DT and CD31 mRNA levels in the ASO arterial endothelium (n = 18). F. Correlation between MAGOH-DT and α-SMA mRNA levels in the ASO arterial endothelium (n = 18). For A-D, n = 3 independent experiments. *$P < 0.05$, **$P < 0.01$, ***$P < 0.001$, ****$P < 0.0001$; ns, not significant.

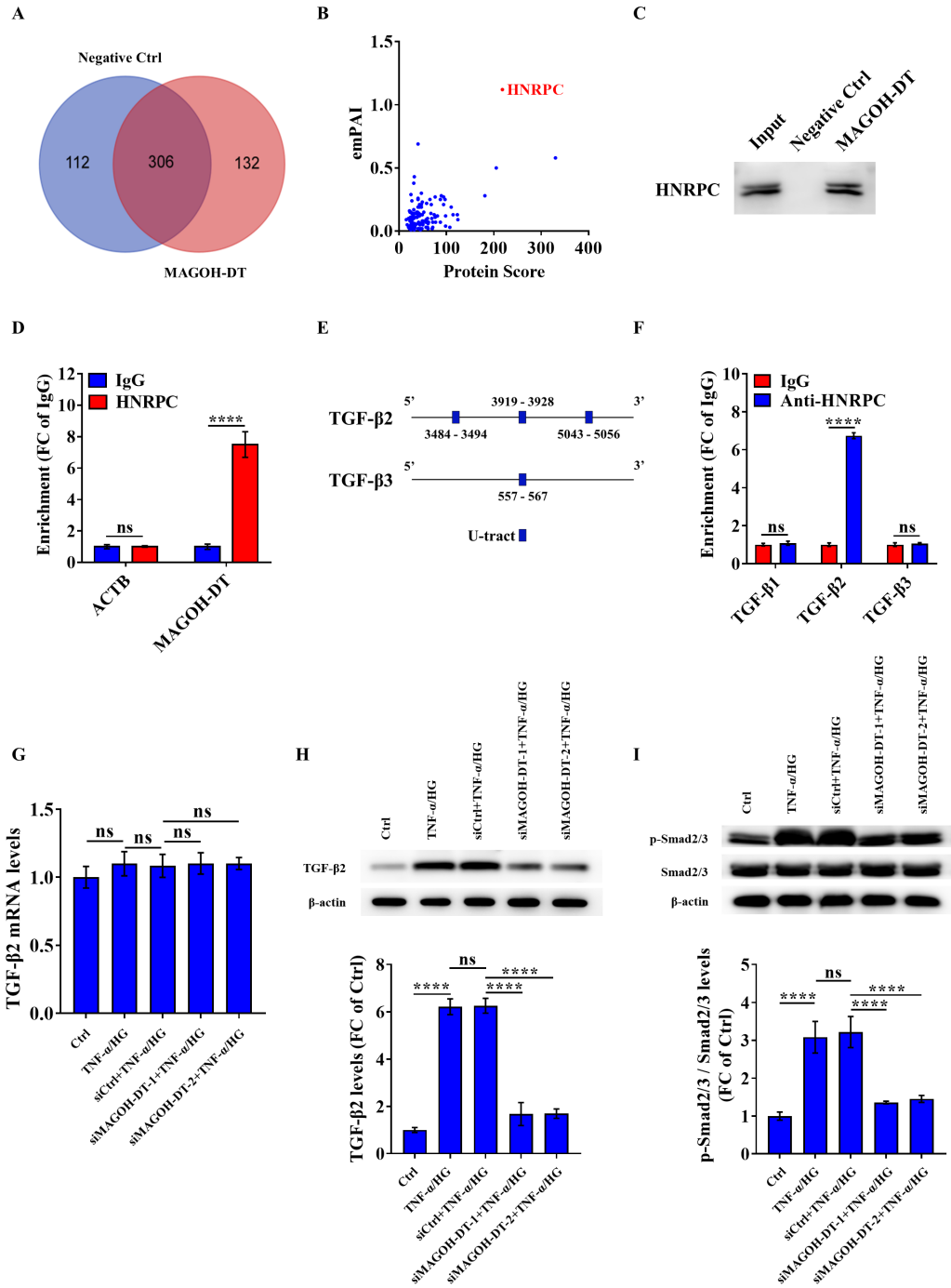

Fig. 4. TNF-α/HG upregulated MAGOH-DT to promote TGF-β2 translation by promoting the interaction between the HNRPC protein and TGF-β2 mRNA.

A. Venn diagram showing the proteins bound to the MAGOH-DT probe or negative control probe in HUVECs after RNA pull-down. B. Scatter plot showing proteins specifically bound to MAGOH-DT. C. Western blot after RNA pull-down demonstrated that MAGOH-DT bound to HNRPC in HUVECs. D. RIP assays confirmed the interaction between MAGOH-DT and HNRPC in HUVECs. ACTB was used as a negative control. E. U-tracts from the mRNA sequences of TGF-β2 and TGF-β3. F. The binding of the Vigilin protein to the TGF-β1, TGF-β2, or TGF-β3 mRNA in HUVECs was determined by RIP assays. G. RT-qPCR was used to determine the mRNA levels of TGF-β2 in HUVECs treated with TNF-α (100 ng/mL) plus HG for 48 hours after MAGOH-DT was knocked down. H. Western blot analysis of TGF-β2 in HUVECs treated with TNF-α (100 ng/mL) plus HG for 48 hours after knocking down MAGOH-DT. Representative plots (top) and quantifications (bottom) are shown. I. Western blot analysis of phospho-Smad2/3, Smad2/3 and GAPDH in HUVECs treated with TNF-α (100 ng/mL) plus HG for 48 hours after knocking down MAGOH-DT. Representative plots (top) and quantifications (bottom) are shown. For B-D and F-I, n = 3 independent experiments. ****$P < 0.0001$; ns, not significant.

to increase the interaction between HNRPC and TGF-β2 mRNA, thus promoting TGF-β2 translation.

TGF-β/Smad signaling pathway plays a pivotal role in mediating EndMT (Dejana et al. 2017; Pardali et al. 2017; Xiao and Dudley 2017). Therefore, we detected the phosphorylation of Smad2/3 (p-Smad2/3), an indicator of TGF-β/Smad signaling activity, to evaluate the impact of TNF-α/HG-induced MAGOH-DT on TGF-β/Smad activation. TNF-α/HG treatment significantly enhanced Smad2/3 phosphorylation in HUVECs, which was inhibited by MAGOH-DT knockdown (all $P < 0.0001$) (Fig. 4I).

These findings suggest that TNF-α/HG-induced MAGOH-DT binds to promote TGF-β2 expression, leading to the activation of TGF-β/Smad signaling and the induction of EndMT.

Discussion

In ASO, endothelial dysfunction serves as a critical and persistent contributor to the development of arterial lesions, with a strong link to inflammatory mediators derived from either systemic inflammation or the autonomous generation within arterial lesions. Prior research indicates that TNF-α plays a significant role in triggering EndMT, thereby accelerating the progression of atherosclerosis (Cao et al. 2020). Therapeutic strategies focused on anti-inflammation have shown efficacy in safeguarding endothelial functions and diminishing the occurrence of vascular incidents (Späh 2008). Furthermore, diabetes mellitus emerges as a pivotal risk factor for ASO, distinguished by persistently elevated levels of blood glucose. Under hyperglycemic conditions, endothelial cells are prone to undergo EndMT, leading to a compromise in their physiological roles (Thomas et al. 2019; Lu et al. 2021). This dysfunctionality in endothelial cells, characterized by a shift towards a mesenchymal phenotype, facilitates the undue build-up of extracellular matrix proteins within the affected vessels.

In this study, we identified a novel long noncoding RNA named MAGOH-DT, which exhibited upregulation in the vessels of patients with ASO and participated in the process of TNF-α/HG-induced EndMT. Building on the foundation laid by previous research, which has demonstrated that TNF-α and HG can independently influence TGF-β expression through distinct signaling pathways to foster EndMT (Souilhol et al. 2018), our findings reveal that both TNF-α and HG upregulate MAGOH-DT expression. This upregulation facilitates the interaction between HNRPC protein and TGF-β2 mRNA, culminating in an increased expression of TGF-β2 protein. The TGF-β/Smad signaling axis is instrumental in the initiation and propagation of EndMT. Notably, while all three isoforms of TGF-β are implicated in EndMT induction, TGF-β2 emerges as the most potent inducer (Sabbineni et al. 2018). The induction of EndMT by TGF-β1 and TGF-β3 necessitates paracrine-mediated stimulation of TGF-β2 production (Sabbineni et al. 2018). MAGOH-DT thus emerges as a critical mediator for both TNF-α and HG stimuli, underscoring its potential therapeutic value in managing EndMT associated with hyperglycemic and proinflammatory conditions. Beyond its role in regulating endothelial cell proliferation, migration, and tube formation, EndMT is implicated in enhancing the secretion of extracellular matrix proteins and upregulating various leukocyte adhesion molecules. These actions contribute to matrix stiffening and the infiltration of monocytes or macrophages (Chen et al. 2015; Souilhol et al. 2018). Although silencing MAGOH-DT does not rectify the altered proliferation and migration of endothelial cells, it significantly mitigates EndMT. Furthermore, our research indicates that TNF-α/HG stimulation augments the expression of endothelial adhesion factors and bolsters monocyte adherence to endothelial cells. However, the knockdown of MAGOH-DT, HNRPC, or both attenuates the effects induced by TNF-α/HG. Consequently, the silencing of MAGOH-DT may offer a novel strategy to alleviate arterial inflammation, thereby potentially curbing the progression of atherosclerosis. This avenue warrants further exploration in future studies.

HNRPC is predominantly found in the endothelial cells of healthy arteries, whereas its presence is notably reduced in the smooth muscle cells. Contrastingly, in the context of atherosclerotic lesions characterized by intimal hyperplasia, HNRPC expression is significantly elevated, with the intimal layer being largely composed of SMA+ cells (Panchenko et al. 2009). These SMA+ cells might originate not solely from the proliferation of activated smooth muscle cells via HNRPC-involved signaling pathways but could also be myofibroblasts that have differentiated from endothelial cells through EndMT. Literature reveals that the long noncoding RNA CEBPA-DT is capable of binding to HNRPC, facilitating the cytoplasmic relocation of HNRPC. This, in turn, enhances the interaction between HNRPC and DDR2 mRNA, leading to an upsurge in DDR2 expression (Cai et al. 2022). Additionally, HNRPC functions as an RNA-binding protein that can elevate mRNA translation efficiency by attaching to its 3′-untranslated region (3′-UTR) (Navickas et al. 2023). A pivotal discovery of our research is that the silencing of either MAGOH-DT or HNRPC curtails the TNF-α/HG-induced increase in TGF-β2 protein levels without altering its mRNA abundance. This suggests that MAGOH-DT might collaborate with HNRPC in a manner analogous to CEBPA-DT, by promoting the cytoplasmic translocation of HNRPC and facilitating its binding to TGF-β2 mRNA. This interaction is hypothesized to enhance TGF-β2 translation. The elucidation of this proposed mechanism merits further investigation.

Conclusion

In conclusion, MAGOH-DT emerges as a crucial intermediary in the process of TNF-α/HG-induced EndMT. This investigation offers preliminary evidence of a shared pathway between hyperglycemia and inflammation in endo-

thelial cell dysfunction. Consequently, MAGOH-DT represents a promising therapeutic target for ASO, especially in patients suffering from diabetes mellitus, highlighting its potential significance in the development of targeted treatments for vascular diseases.

Acknowledgments

This research was financially supported by the National Natural Science Foundation of China (Grant 82200544) and the fellowship of China Postdoctoral Science Foundation (Grant 2022M723645).

K.J.W., Y.X.Z., Z.W.M. and W.B.W. conceived and designed the study. K.J.W., Y.X.Z., Z.W.M. and W.B.W. performed the experiments. K.J.W., Z.W.M. and W.B.W. wrote the manuscript. K.J.W., Y.X.Z., Z.W.M., Z.L.L., M.W., R.W., Z.C.W., G.Q.C. and W.B.W. generated or analyzed the data. G.Q.C. and W.B.W. supervised the project and revised the manuscript.

Conflict of Interest

The authors declare no conflict of interest.

References

Adjuto-Saccone, M., Soubeyran, P., Garcia, J., Audebert, S., Camoin, L., Rubis, M., Roques, J., Binetruy, B., Iovanna, J.L. & Tournaire, R. (2021) TNF-α induces endothelial-mesenchymal transition promoting stromal development of pancreatic adenocarcinoma. *Cell Death Dis.*, **12**, 649.

Alvandi, Z. & Bischoff, J. (2021) Endothelial-Mesenchymal Transition in Cardiovascular Disease. *Arterioscler. Thromb. Vasc. Biol.*, **41**, 2357-2369.

Cai, Y., Lyu, T., Li, H., Liu, C., Xie, K., Xu, L., Li, W., Liu, H., Zhu, J., Lyu, Y., Feng, X., Lan, T., Yang, J. & Wu, H. (2022) LncRNA CEBPA-DT promotes liver cancer metastasis through DDR2/β-catenin activation via interacting with hnRNPC. *J. Exp. Clin. Cancer Res.*, **41**, 335.

Cao, T., Jiang, Y., Li, D., Sun, X., Zhang, Y., Qin, L., Tellides, G., Taylor, H.S. & Huang, Y. (2020) H19/TET1 axis promotes TGF-β signaling linked to endothelial-to-mesenchymal transition. *FASEB J.*, **34**, 8625-8640.

Chen, L., Shang, C., Wang, B., Wang, G., Jin, Z., Yao, F., Yue, Z., Bai, L., Wang, R., Zhao, S., Liu, E. & Wang, W. (2021a) HDAC3 inhibitor suppresses endothelial-to-mesenchymal transition via modulating inflammatory response in atherosclerosis. *Biochem. Pharmacol.*, **192**, 114716.

Chen, L., Zhang, X., Jiang, F., Yin, Z., Xue, J., Ruan, C. & Xie, L. (2021b) Therapeutic Effects of Interventional Therapy and Conservative Therapy on Lower Extremity Arteriosclerosis Obliterans and Risk Factors for Prognosis. *Artery Research*, ***27***, 101-106.

Chen, P.Y., Qin, L., Baeyens, N., Li, G., Afolabi, T., Budatha, M., Tellides, G., Schwartz, M.A. & Simons, M. (2015) Endothelial-to-mesenchymal transition drives atherosclerosis progression. *J. Clin. Invest.*, **125**, 4514-4528.

Ciavarella, C., Motta, I., Vasuri, F., Fittipaldi, S., Valente, S., Pollutri, D., Ricci, F., Gargiulo, M. & Pasquinelli, G. (2021) Involvement of miR-30a-5p and miR-30d in Endothelial to Mesenchymal Transition and Early Osteogenic Commitment under Inflammatory Stress in HUVEC. *Biomolecules*, **11**, 226.

Cieniková, Z., Damberger, F.F., Hall, J., Allain, F.H. & Maris, C. (2014) Structural and mechanistic insights into poly(uridine) tract recognition by the hnRNP C RNA recognition motif. *J. Am. Chem. Soc.*, **136**, 14536-14544.

Cieniková, Z., Jayne, S., Damberger, F.F., Allain, F.H. & Maris, C. (2015) Evidence for cooperative tandem binding of hnRNP C RRMs in mRNA processing. *RNA*, **21**, 1931-1942.

Collado, A., Gan, L., Tengbom, J., Kontidou, E., Pernow, J. & Zhou, Z. (2023) Extracellular vesicles and their non-coding RNA cargos: Emerging players in cardiovascular disease. *J. Physiol.*, **601**, 4989-5009.

Dantsuji, S., Ohno, M. & Taniguchi, I. (2023) The hnRNP C tetramer binds to CBC on mRNA and impedes PHAX recruitment for the classification of RNA polymerase II transcripts. *Nucleic Acids Res.*, **51**, 1393-1408.

Dejana, E., Hirschi, K.K. & Simons, M. (2017) The molecular basis of endothelial cell plasticity. *Nat. Commun.*, **8**, 14361.

Haemmig, S., Yang, D., Sun, X., Das, D., Ghaffari, S., Molinaro, R., Chen, L., Deng, Y., Freeman, D., Moullan, N., Tesmenitsky, Y., Wara, A., Simion, V., Shvartz, E., Lee, J.F., et al. (2020) Long noncoding RNA SNHG12 integrates a DNA-PK-mediated DNA damage response and vascular senescence. *Sci. Transl. Med.*, **12**, eaaw1868.

Hong, L., Li, F., Tang, C., Li, L., Sun, L., Li, X. & Zhu, L. (2020) Semaphorin 7A promotes endothelial to mesenchymal transition through ATF3 mediated TGF-beta2/Smad signaling. *Cell Death Dis.*, **11**, 695.

Krappinger, J.C., Bonstingl, L., Pansy, K., Sallinger, K., Wreglesworth, N.I., Grinninger, L., Deutsch, A., El-Heliebi, A., Kroneis, T., McFarlane, R.J., Sensen, C.W. & Feichtinger, J. (2021) Non-coding Natural Antisense Transcripts: Analysis and Application. *J. Biotechnol.*, **340**, 75-101.

Li, D., Yang, C., Li, X., Ji, G. & Zhu, L. (2008) Sense and antisense OsDof12 transcripts in rice. *BMC Mol. Biol.*, **9**, 80.

Li, H.M., Mo, Z.W., Peng, Y.M., Li, Y., Dai, W.P., Yuan, H.Y., Chang, F.J., Wang, T.T., Wang, M., Hu, K.H., Li, X.D., Ning, D.S., Chen, Y.T., Song, Y.K., Lu, X.L., et al. (2020) Angiogenic and Antiangiogenic mechanisms of high density lipoprotein from healthy subjects and coronary artery diseases patients. *Redox Biol.*, **36**, 101642.

Lu, L., Li, X., Zhong, Z., Zhou, W., Zhou, D., Zhu, M. & Miao, C. (2021) KMT5A downregulation participated in High Glucose-mediated EndMT via Upregulation of ENO1 Expression in Diabetic Nephropathy. *Int. J. Biol. Sci.*, **17**, 4093-4107.

Ma, J., Sanchez-Duffhues, G., Goumans, M.J. & Ten Dijke, P. (2020) TGF-beta-Induced Endothelial to Mesenchymal Transition in Disease and Tissue Engineering. *Front. Cell Dev. Biol.*, **8**, 260.

Mineo, C. (2020) Lipoprotein receptor signalling in atherosclerosis. *Cardiovasc. Res.*, **116**, 1254-1274.

Mo, L., Meng, L., Huang, Z., Yi, L., Yang, N. & Li, G. (2022) An analysis of the role of HnRNP C dysregulation in cancers. *Biomark. Res.*, **10**, 19.

Mo, Z.W., Peng, Y.M., Zhang, Y.X., Li, Y., Kang, B.A., Chen, Y.T., Li, L., Sorci-Thomas, M.G., Lin, Y.J., Cao, Y., Chen, S., Liu, Z.L., Gao, J.J., Huang, Z.P., Zhou, J.G., et al. (2023) High-density lipoprotein regulates angiogenesis by long non-coding RNA HDRACA. *Signal Transduct. Target. Ther.*, **8**, 299.

Nasim, S., Wylie-Sears, J., Gao, X., Peng, Q., Zhu, B., Chen, K., Chen, H. & Bischoff, J. (2023) CD45 Is Sufficient to Initiate Endothelial-to-Mesenchymal Transition in Human Endothelial Cells-Brief Report. *Arterioscler. Thromb. Vasc. Biol.*, **43**, e124-e131.

Navickas, A., Asgharian, H., Winkler, J., Fish, L., Garcia, K., Markett, D., Dodel, M., Culbertson, B., Miglani, S., Joshi, T., Yin, K., Nguyen, P., Zhang, S., Stevers, N., Hwang, H.W., et al. (2023) An mRNA processing pathway suppresses metastasis by governing translational control from the nucleus. *Nat. Cell Biol.*, **25**, 892-903.

Palazzo, A.F. & Lee, E.S. (2015) Non-coding RNA: what is functional and what is junk? *Front. Genet.*, **6**, 2.

Panchenko, M.P., Silva, N. & Stone, J.R. (2009) Up-regulation of a hydrogen peroxide-responsive pre-mRNA binding protein in atherosclerosis and intimal hyperplasia. *Cardiovasc. Pathol.*,

18, 167-172.
Pardali, E., Sanchez-Duffhues, G., Gomez-Puerto, M.C. & Ten Dijke, P. (2017) TGF-beta-Induced Endothelial-Mesenchymal Transition in Fibrotic Diseases. *Int. J. Mol. Sci.*, **18**, 2157.
Sabbineni, H., Verma, A. & Somanath, P.R. (2018) Isoform-specific effects of transforming growth factor beta on endothelial-to-mesenchymal transition. *J. Cell. Physiol.*, **233**, 8418-8428.
Souilhol, C., Harmsen, M.C., Evans, P.C. & Krenning, G. (2018) Endothelial-mesenchymal transition in atherosclerosis. *Cardiovasc. Res.*, **114**, 565-577.
Späh, F. (2008) Inflammation in atherosclerosis and psoriasis: common pathogenic mechanisms and the potential for an integrated treatment approach. *Br. J. Dermatol.*, **159** Suppl 2, 10-17.
Thomas, A.A., Biswas, S., Feng, B., Chen, S., Gonder, J. & Chakrabarti, S. (2019) lncRNA H19 prevents endothelial-mesenchymal transition in diabetic retinopathy. *Diabetologia*, **62**, 517-530.
Wu, G., Cai, J., Han, Y., Chen, J., Huang, Z.P., Chen, C., Cai, Y., Huang, H., Yang, Y., Liu, Y., Xu, Z., He, D., Zhang, X., Hu, X., Pinello, L., et al. (2014) LincRNA-p21 regulates neointima formation, vascular smooth muscle cell proliferation, apoptosis, and atherosclerosis by enhancing p53 activity. *Circulation*, **130**, 1452-1465.
Xiao, L. & Dudley, A.C. (2017) Fine-tuning vascular fate during endothelial-mesenchymal transition. *J. Pathol.*, **241**, 25-35.
Yuan, Y.Y., Cao, W.D., Zhang, X.H., Du, R.X., Wang, X.Q., Li, J., Chen, J., Yang, J.Z. & Chen, J.Q. (2023) Application of E-coach chronic disease management model in rehabilitation management of patients with arteriosclerosis obliterans. *J. Health Popul. Nutr.*, **42**, 115.
Zhang, Y., Liu, D., Chen, X., Li, J., Li, L., Bian, Z., Sun, F., Lu, J., Yin, Y., Cai, X., Sun, Q., Wang, K., Ba, Y., Wang, Q., Wang, D., et al. (2010) Secreted monocytic miR-150 enhances targeted endothelial cell migration. *Mol. Cell*, **39**, 133-144.
Zhao, H., Zhuo, T., Hao, X., Fan, X. & Zhao, P. (2022) Effect of diabetes on the prognosis, serum inflammatory factors, and quality of life of patients with lower extremity arteriosclerosis obliterans after vascular intervention: a retrospective comparative cohort study. *Ann. Palliat. Med.*, **11**, 2720-2729.
Zhao, Y., Hou, Y., Zhao, C., Liu, F., Luan, Y., Jing, L., Li, X., Zhu, M. & Zhao, S. (2016) Cis-Natural Antisense Transcripts Are Mainly Co-expressed with Their Sense Transcripts and Primarily Related to Energy Metabolic Pathways during Muscle Development. *Int. J. Biol. Sci.*, **12**, 1010-1021.

Supplementary Files

Please find supplementary file(s);
https://doi.org/10.1620/tjem.2024.J031